Earth and Planetary Science Letters 288 (2009) 84–95

Contents lists available at ScienceDirect

Earth and Planetary Science Letters

journal homepage: www.elsevier.com/locate/epsl

Centrifuge assisted percolation of Fe–S melts in partially molten peridotite: Time constraints for planetary core formation

N. Bagdassarov [a,b,*], G. Solferino [b], G.J. Golabek [a,c], M.W. Schmidt [b]

[a] Institute for Geosciences, Altenhöferallee 1, University Frankfurt, D-60438 Frankfurt, Germany
[b] Institute for Mineralogy and Petrology, Clausiusstrasse 25, ETH Zürich, CH-8092 Zürich, Switzerland
[c] Institute for Geophysics, Sonneggstrasse 5, ETH Zürich, CH-8092 Zürich, Switzerland

ARTICLE INFO

Article history:
Received 9 January 2009
Received in revised form 3 September 2009
Accepted 7 September 2009
Available online 1 October 2009

Editor: T. Spohn

Keywords:
accretion
differentiation
percolation
Vesta
Mars
Earth

ABSTRACT

The mechanism which segregates molten Fe–S into metallic cores of planetary bodies is still not fully understood. Due to the high interfacial energy and wetting angle between Fe–S melts and silicate mantle minerals, the continuous percolative flow of such melts cannot be efficient for the core segregation in planetary bodies. A series of percolation experiments has been realized on a partially molten fertile garnet peridotite, employing a centrifuging piston cylinder. A high temperature garnet peridotite with Mg# ~0.90 composed of 60 vol.% olivine, 15 vol.% orthopyroxene, 6 vol.% clinopyroxene and 19 vol.% garnet has been used as the silicate matrix. Peridotite powders with the 100–200 or 20–30 μm grain size were mixed with 5–30 vol.% Fe–S of eutectic composition $Fe_{70}S_{30}$. The aggregates were centrifuged at 500–700 g at temperatures below and above the melting point of the peridotite. The centrifuge experiments revealed a negligible percolation of Fe–S melts through the unmolten peridotite matrix. Only at $T > 1260$ °C, i.e. above the solidus of the peridotite, and starting with 5 vol.% of $Fe_{70}S_{30}$ the vertical melt gradient achieved 1–2 vol.%/mm. In samples with 15 vol.% $Fe_{70}S_{30}$ the vertical separation achieved 2–2.5 vol.%/mm after 10 h of centrifuging at 500 g. An increase in the degree of partial silicate melting in the peridotite leads to an increase of the Fe–S separation rate from the peridotite matrix. Fe–S contents >10 vol.% cause an increase of the Fe–S melt droplet size and of the effective percolation velocity of Fe–S melt. A threshold dividing fast (>10 cm per year) and slow percolations (<1 mm per year) of Fe_S melt is found around 14–15 vol.% of $Fe_{70}S_{30}$. The experimentally determined permeabilities of Fe–S melt in the unmolten peridotite with 7–10 vol.% of $Fe_{70}S_{30}$ melt are 10^{-18}–10^{-19} m^2, which is 2–3 orders of magnitude lower than the values calculated previously from static experiments. The presence of the silicate melt increases the segregation velocity of Fe–S melt in a partially molten peridotite by more than one order of magnitude with respect to the unmolten peridotite matrix. This could provide an effective segregation of Fe–S melt in a planetary mantle down to 2.5 vol.% of residual Fe–S melt. The extremely slow percolation of Fe–S melt in the absence of the partial silicate melting precludes a scenario of metallic core formation *via* percolation before temperatures allow a substantial partial melting of mantle silicates in planetary bodies.

1. Introduction

One of the most intriguing questions dealing with the formation of the Earth and planetary bodies is the time scale and mechanism of metal–silicate differentiation and the formation time of metallic cores. The current understanding of the accretion time of terrestrial planets indicates that intensive accretion and differentiation of the large terrestrial planets took place simultaneously over some tens of millions of years after the start of the solar system (Chambers, 2004). Small terrestrial bodies, like Asteroid 4 Vesta, seem to have formed early, i.e. within the first 1–2 Ma (Greenwood et al., 2005). Numerical *N* body simulations indicate that the accretion of larger bodies like Mars took about 0.1–10 Ma (Chambers, 2004; Nimmo and Kleine, 2007). The Earth's accretion was more protracted, and the results of the *N* body simulations permit to infer a time of c. 100 Ma until the accretion was completed (Canup and Agnor, 2000). This is in a good agreement with the isotopic results from the *Pb–Pb* system. The age of the refractory materials in CAI meteorites (4.568 Ga), thought to correspond to the time of the solar nebular formation, and the age of the Earth obtained from *Pb–Pb* chronometry of MORBs (<4.45 Ga), yield a time span for the Earth's core formation no longer than 100 Ma (Allègre et al., 1995, 2008). Using the closure time of the *I–Pb–Xe* isotope system, Wetherill (1975) estimated the *Xe* closure age of the Earth to be 113–127 Ma, whereas Allègre et al. (1995) obtained 105–110 Ma for the age of the Earth at the time when the growing planet started to retain its atmosphere.

* Corresponding author. Institute for Geosciences, Altenhöferallee 1, University Frankfurt, D-60438 Frankfurt, Germany.
E-mail address: nickbagd@geophysik.uni-frankfurt.de (N. Bagdassarov).

0012-821X/$ – see front matter © 2009 Elsevier B.V. All rights reserved.
doi:10.1016/j.epsl.2009.09.010

Earlier results on the core formation in planetary bodies from Hf–W chronometry infer a much shorter time (Kleine et al. 2002; Kleine et al. 2004, 2005). The duration of the metallic core formation assumed as a single event has been estimated as 5, 13, and 33 Ma for Vesta, Mars, and the Earth, respectively (Kleine et al., 2002). New measurements of $^{142}Nd/^{144}Nd$ in chondrites and the revisited superchondritic terrestrial ε^{142}_{Nd} of 20 may be explained by the presence of a high Sm/Nd reservoir not later than 4.537 Ga ago, i.e. 30 Ma after the solar system formation (Boyet and Carlson, 2005). The early timing of the Earth's core differentiation has been critically discussed by Wood and Halliday (2005), Wade and Wood (2005), Wood et al. (2006), Halliday (2008), and Allègre et al. (2008). The core formation time of Kleine et al. (2002) is based on the assumption of a total equilibrium between an impactor material and the bulk silicate Earth (BSE). Such rapid equilibration of an incoming material in a planetary body assumes an effective percolation of iron melts in a permeable solid matrix or a rapid sinking of molten iron in partially molten silicates. If the proto-Earth was not melted at the early accretion stage and the incoming flux of molten metallic sulphide from the bombardment process was still substantial, the fast equilibration would imply an effective transport of the Fe–S melt through the silicate mantle in a grain size length scale. An isotopic equilibration requires that the iron and silicate phases are mixed at a small length scale and that their residence timescale is comparable with their diffusion timescale (Nimmo and Agnor, 2006). Consequently, equilibration of Hf–W between the metal melt and BSE might not be fully achieved, if their relative motion is fast (~1 m/a). This could result in the observed excess of ^{182}W ($\varepsilon_W \sim 1.9$) in the BSE relative to chondrites ($\varepsilon_W \sim 0$). Hf–W chronometry would then indicate a time span intermediate between the segregation time of the iron melt in the projectiles and the true core formation time of the Earth (Wood and Halliday, 2005; Allègre et al., 2008). The observed excesses of ^{182}W in a planetary body are difficult to interpret, if the isotopic re-equilibration scenario of impactor and target is not known precisely (Nimmo and Agnor, 2006). A fast merging of the impactor core and the mantle into the target mantle and core, or a complete equilibration of the impactor with the target mantle may result in a mantle excess of ^{182}W, and consequently, the derived core formation time would then be underestimated (Nimmo and Agnor, 2006).

This argument is also based on the presumption that the mantle silicates, even without partial melting, let the metallic melt segregate due to a non-zero permeability at the early stage of accretion. Numerous dihedral angle measurements of the Fe–S melt in silicates (Lee and Agee, 1996; Minarik et al., 1996; Ballhaus and Ellis, 1996; Gaetani and Grove, 1999; Terasaki et al., 2007; Walte et al., 2007), yielded wetting angles larger than 60°. The dihedral angle varies from 90° at 43 at.% of O + S to 60° at 53 at.% of O + S in a metallic melt at 3–4 GPa (Minarik et al. 1996). Recent experiments on dihedral angles between Fe–S–O melts and olivine crystals with the Mg# of 0.90–0.76 (Terasaki et al., 2008) suggest a significant pressure dependence of the wetting properties of Fe–S–O melts. At low pressures (<2–3 GPa) and oxidizing conditions (>25–20 at.% O) the wetting angle is <60°, which allows the percolation flow of Fe–S–O melts in planetary bodies with relatively small size (Terasaki et al., 2008). A decrease of the Mg# of olivine resulted in a small decrease of the wetting angle. At high pressures, even in oxidizing conditions, wetting angles remain higher than the threshold for an interconnected network of the melt which precludes an effective percolation mechanism for the Fe–S transport into the core.

Experimental support for a non-zero permeability of mantle silicates to the Fe–S melt flow has been obtained only from the electrical conductivity of olivine and Fe–S mixtures (Yoshino et al., 2003, 2004) indicating that even at about 6 vol.% Fe–S and temperatures below the peridotite solidus Fe–S melts become interconnected. This result is supported by a 3D synchrotron radiation tomography of statically annealed Fe–Ni–S alloys (Roberts et al., 2007). From the topology of Fe–S melt pockets, the permeability of the silicate matrix was calculated to be 10^{-18}–10^{-19} m^2 at 1 vol.% and to be 10^{-13} m^2 at 13 vol.% of Fe–S melt. In a partially molten peridotite, the interconnectivity threshold of the Fe–S melt in a peridotite matrix has been estimated to be 13 ± 2 vol.% Fe–S through electrical conductivity measurements (Yoshino et al. 2004). Walte et al. (2007) demonstrated that an interconnected network of the Fe–S melt in a silicate matrix is not stable due to the high dihedral angle of >60° and should pinch off in long duration experiments. Walte et al. (2007) also show that the very limited mobility of high wetting angle liquid pockets is possible only due to slight adjustments of the pocket shape and the shape of surrounding solid grains during textural maturation and the related flow of the melt phase.

In this study we investigate the mechanism of the Fe–S melt segregation in a silicate matrix and test the plausibility of a percolation flow with a direct experimental simulation of this segregation process in peridotite + Fe–S samples. We performed a series of segregation experiments with the centrifuging piston cylinder at ETH (Schmidt et al., 2006). The main goal was to achieve a gravitational separation of the molten Fe–S alloy from a silicate matrix and to measure melt segregation velocities as a function of metal and silicate melt contents in a peridotite matrix under compaction.

2. Theoretical background for the centrifuge experiments

Material flows in nature and in dynamic laboratory experiments are similar, provided that they are geometrically similar and their dimensionless numbers are close to each other. If a dynamic process may be described by a functional dependency of one dimensionless number on another, we can determine this relationship by performing experiments on small scale objects in short time scale experiments and then extrapolate our functional dependency to the geological length and time scales. Some parameters involved in dimensionless numbers, such as mass and energy, are difficult to vary over a wide range. Gravitational acceleration however is involved in many dimensionless numbers characterizing dynamic processes during the planetary accretion, e.g. the percolation flow, droplets raining in a magma ocean, and the flow in intergranular channels. By imposing a centrifugal acceleration of 1000 g on an experimental system, these segregation processes occur on a proportionally shorter time scale, as the centrifugal acceleration replaces gravity acceleration (Bagdassarov et al., 1996a,b).

The percolation rate of the metal melt in a peridotite matrix may be calculated from the equation of mass conservation (McKenzie, 1984; Yang, 2001). Assuming a time and depth independent melt density ρ_f and the conservation of Fe–S mass M, then

$$\rho_f\left(\frac{\partial\varphi}{\partial t} + \vec{\nabla}\cdot(\varphi\cdot\vec{v}_f)\right) = \frac{dM}{dt} = 0, \quad (1)$$

where φ is the melt fraction, and v_f the segregation velocity of the melt. Here and below φ is the melt fraction. For a one-dimensional flow with a downward segregation direction z

$$\frac{\partial\varphi}{\partial t} = -\frac{\partial(\varphi\cdot v_f)}{\partial z} = \frac{\partial([1-\varphi]\cdot v_s)}{\partial z}. \quad (2)$$

In Eq. (2) v_s is the solid matrix velocity. The z-coordinate in the experiments described below is the coordinate along the axis of the cylindrical sample, which is parallel to the centrifugal force. In a natural system, this axis would correspond to the vertical direction (hence z) and the length of the sample along this axis is hitherto referred to as the height of the sample. The centrifuge acceleration acts along the z-coordinate in the direction from the top to the bottom

of the centrifuged capsules. The conservation of momentum can be described by the 1D Darcy's equation as follows

$$\varphi\cdot(v_f - v_s)\cdot\frac{\mu}{\kappa} = \eta\frac{\partial^2 v_s}{\partial z^2} + \Delta\rho\cdot g, \quad (3)$$

where k is the permeability of the solid matrix, μ is the shear viscosity of the percolating fluid phase, and η is the bulk viscosity of the matrix (McKenzie, 1984). In Eq. (3) the pressure difference between the solid and fluid phase has been replaced by a product of the matrix bulk viscosity and gradient of the solid phase velocity, i.e. the compaction of the solid matrix is assumed as a pure viscous mechanism (Sumita et al., 1996). The left-hand side in Eq. (3) is the viscous friction of flow through the solid matrix, the first term in the right side is the viscous resistance to the matrix compaction and the second term is the buoyancy (Sumita et al., 1996).

Let us assume a laboratory experiment on compaction of a solid matrix and melt segregation with the centrifuge acceleration 1000g. For $t=0$, $\varphi=\varphi_0$ is assumed to be constant and the melt fraction distributed homogeneously over the height or a vertical z-axe of a cylindrical sample which is directed along the radius of the sample gyration. In a laboratory sample the porosity at the barycentre remains equal to the initial or average porosity. In the case $h \ll \delta_c$ the approximate solutions of the 1D-compaction problem between the two impermeable boundaries are as follows $v_s(z) \approx -v_0\cdot\varphi\cdot\frac{z}{\delta_c^2}\cdot(h-\frac{z}{2})$, and $v_s = -\frac{\varphi}{1-\varphi}\cdot v_f$ (McKenzie, 1984). The velocity $v_0 = \frac{\kappa}{\mu}\cdot\frac{1-\varphi}{\varphi}\cdot\Delta\rho\cdot g$ is the scale velocity which corresponds to the case $\delta_c=0$ or Darcian flow with constant porosity and without compaction. Assuming a shear viscosity of the peridotite matrix of 10^{14} Pa s at 1150 °C and the grain size c. 20 μm (Zimmerman and Kohlstedt, 2004) is equal to the bulk viscosity η, the permeability k is of 10^{-15} m² at 10% of melt porosity and 5×10^{-18} m² at 1% of melt porosity (Roberts et al., 2007) and the viscosity μ of Fe–S melt of 10^{-2} Pa s (Alfè and Gillan, 1998; Urakawa et al., 2001), the compaction length is about $\delta_c \sim 0.2$–1 m (Ricard et al., 2001). The typical size of the laboratory sample H is ~2 mm, which is much smaller than the compaction length δ_c. The pore-solid matrix deformation factor is $H/\delta_c \sim 10^{-2}$–10^{-4}. In real centrifuge experiments, the condition of impermeable boundaries was not realized. The samples were encapsulated in graphite and during the experiment they were under 1 GPa of hydrostatic pressure. The inspection of samples after centrifuge experiments demonstrates the absence of silicate melt collection on the top and Fe–S melt on the bottom and any noticeable deformation of sample was not observed. Thus, we may regard the resulting density driven flow realized in centrifuge experiments as a Darcian flow at a quasi constant melt pressure gradient. As the porosity and melt pressure gradients are constant during a short time t ($\sim\tau_0 = \frac{\delta_c}{v_0\cdot(1-\varphi)}$, McKenzie, 1984) after the start of the experiment, it follows that the melt velocity at the barycentre is likewise constant, at least for the experimental time scale, $v_f = v_0\cdot(1=\varphi)$ and $v_s = -v_0\cdot\varphi$.

The substitution of differentials by finite quotient differences in Eq. (2) yields an equation that can be applied to measurements of the Fe–S melt abundance in a sample having the height H after a time Δt of segregation,

$$v_f = \frac{1}{\overline{\varphi}\cdot\Delta t}\int_0^H \Delta\varphi\cdot dZ \approx \frac{\Delta\varphi\cdot H}{2\cdot\overline{\varphi}\cdot\Delta t}, \quad (4)$$

where $\overline{\varphi}$ is the average melt porosity at $t=0$. The factor 0.5 in Eq. (4) is due to the integration of a linear function $\Delta\varphi(z)$. After the centrifugation during the time Δt, the difference $\Delta\varphi$ can be determined between the gravitational top and bottom of the centrifuged sample. Strictly speaking, the segregation velocity in Eq. (4) is the melt velocity relative to the barycentre and not the true physical velocity of the melt phase relative to the solid matrix. In the light of the relatively large error in evaluating v_f from Eq. (4) and the short time of centrifuging, the approximation that the physical flow velocity is equal to the barycentre velocity in Eq. (4) is reasonable.

The question what kind of a density driven flow can be simulated in centrifuge experiments on rocks containing melts remains. A density driven percolative flow due to the compaction of a solid matrix can be either due to a viscous compaction of a solid matrix (effective normal stress across the grain contacts is proportional to the creep rate of a solid matrix) or due to a poroelastic relation, i.e. the relationship between the effective pressure and porosity (Yang, 2001). The first case occurs at high pressures and over a long period of time, the second case can be realized due to pure mechanical grain displacements such as sliding along grain contacts and grain rearrangements. By applying a moderate hydrostatic pressure and by increasing the pressure gradient $\Delta\rho\cdot g$ by 2–3 orders of magnitude in centrifuge experiments with the accelerations of 500–1000g, the simulated compaction flow can be a combination of the two mechanisms mentioned above. Walte et al. (2007) showed that due to (i) the large density contrast between silicates and iron, and (ii) the high dihedral angle of the Fe–S melt and the rather low viscosity of Fe–S melts, the flow of Fe–S is dominantly poroelastic. To discriminate these two types of flows from the vertical distribution of the melt phase along a compacted sample is rather difficult. Nevertheless, for a poroelastic compaction the upper part of the samples is characterized by small porosity gradients and the bottom part—by very large porosity gradients. For a viscous compaction, large porosity gradients occur in the upper part and the bottom and middle parts are characterized by an almost constant and small porosity gradient (Yang, 2001).

Mungall and Su (2005) discussed the mobility of Fe–S melts in a partially molten silicate framework. The entry of droplets into capillary throats depends on a product of the size of droplets L and the size of a capillary throat r, and this product should be larger than a^2, where a is the capillary constant and is given by $a^2 = \Delta\rho\cdot g/\gamma_{sl}$, where γ_{sl} is the surface tension between the melt and solid phase. By performing centrifuge experiments, the capillary constant is decreased by the factor (*centrifuge acceleration*/g)$^{1/2}$. Thus, the estimated mobility of Fe–S droplets from the centrifuge experiments may be larger than that under natural conditions and may be regarded as an upper limit of porous flow velocities.

Centrifuging of two phase aggregates in a rotating furnace has been successfully used to model crystal-melt segregation processes at high temperatures and atmospheric pressure (Campbell et al. 1978; Kadik et al. 1989, 1990; Bagdassarov et al., 1996a,b; Lebedev et al., 1999). Recent advances in a high pressure technique permit to centrifuge a small piston cylinder and to quench samples within a few seconds (Schmidt et al., 2006), which makes the laboratory compaction simulation with partially molten rocks much more realistic.

3. Experiments

3.1. Sample preparation

The starting materials used for all experiments were mixtures of a natural fertile garnet peridotite (a xenolith from the Jericho kimberlite, Northern Territories, Canada) with a eutectic mixture of Fe–S. The chemical composition and the equilibration conditions of 1190–1260 °C and 5.85–5.95 GPa for this xenolith were given by Kopylova and Russell (2000). Oxygen fugacity relative to the QFM buffer has been estimated to $\Delta\log(f_{O2}) = -3.2$, the $Fe^{3+}/\Sigma Fe$ in garnet is 0.107 (McCammon and Kopylova, 2004), and the bulk Mg# is 0.896. The xenolith consists of 60 vol.% olivine, 15 vol.% orthopyroxene, 6 vol.% clinopyroxene and 19 vol.% garnet (sample 23-5 from McCammon and Kopylova, 2004). The choice of this peridotite sample was dictated by its low melting point of 1180–1200 °C at 1 GPa (Walter, 2003). The peridotite was crushed and milled in a silicon-nitride mortar to a grain size of first 60–120 μm and after two experiments to 20–30 μm. The grain size distribution of powders has been measured with a laser

particle analyzer, the Mastersizer 2000 (Malvern Instrument Ltd.). The composition of the Fe–S powder is that of the eutectic in the Fe–S system, which is at $Fe_{70}S_{30}$ (wt.%) at 1 GPa (Brett and Bell, 1969). The powder has been prepared from Fe and FeS (99.99% ChemPu®), pressed into pellets, sealed in evacuated quartz tubes at 10^{-3} bar, kept at 1200 °C for 5 h in a vertical furnace, and then quenched in water. The pellets were then crushed and milled under ethanol for 10 min. Final mixtures were prepared from fertile peridotite and Fe–S powders with 7.5, 10, 15, 20 and 50 wt.% of $Fe_{70}S_{30}$ by grounding under ethanol. The dried mixtures were agitated for 10 min to get a maximum of homogenization.

Two reasons led to use a eutectic Fe–S composition: (i) its low melting temperature compared to the silicate phases and (ii) the necessity to have all Fe–S as liquid. (i): The experiments were conducted at 1 GPa and we chose the eutectic composition of Fe–S (27 wt.% of S) corresponding to this pressure. With pressure, the eutectic temperature increases and the S content of the eutectic decreases: at 21 and 40 GPa the melting temperatures are 1070 and 1250 °C, and the eutectic compositions are 15 and 12 wt.% S, respectively (Usselman 1975, Li and Fei 2004, Stewart et al., 2007). Any of these temperatures are more than 100 °C lower than the corresponding solidus of a dry mantle peridotite. Qualitatively, removing S from Fe–S melt would increase the surface tension and the dihedral angle and thus, with increasing pressure, percolation of the Fe–S melt in a silicate matrix becomes less probable (Terasaki et al., 2009). Nevertheless, by adding O to the Fe–S melt or by increasing the Fe-number of the peridotite matrix, the dihedral angle may decrease but will still remain above 60° (Terasaki et al., 2007). (ii): A quantification of the experimental results in the context of this study depends on the metal phase having a unique liquid state. A bulk Fe–S composition within the two phase loop would lead to a silicate melt carrying both rounded and rigid Fe grains and droplets of Fe–S melt, which would have different mechanical properties and segregation behaviour. Furthermore, for a Fe–S composition within the two phase loop, the Fe–S melt would strongly change the S-content with temperatures leading to a further variable in the experiments.

The materials for the centrifuging experiments were sintered in an endloaded piston cylinder (Table 1) using NaCl–Pyrex–graphite–MgO assemblies. For this, the powders were pressed into cylindrical pellets 2 mm in diameter and 2.5 mm in height, encapsulated in graphite, and kept during 65–70 h at 1 GPa and temperatures close and above the melting point of fertile garnet peridotite at 1180–1200 °C (Hirschmann et al., 1999). Garnet is not stable at 1 GPa and recrystallizes in spinel. A microscopic analysis of the sintered samples indicates that this process does not affect the distribution of the Fe–S melts. After the static sintering stage, the cylindrical samples have been loaded in the same graphite capsules into the centrifuging piston cylinder employing the same assembly type and size. The temperature was controlled with a *B*-type thermocouple.

3.2. Centrifuge experiments

The centrifuging piston cylinder basically consists of a rotating table (weight 850 kg) with two apertures in which a small piston cylinder press (c. 42 kg) and a counterweight are placed. The table could be spun to the maximum speed of 2900 rpm, equivalent to 3000 times the Earth's gravitational acceleration (g) at the position of the experimental charge (for technical details, see Schmidt et al. 2006). The maximum applied centrifugal acceleration in this study was 700g (Table 1). The cylindrical samples have been oriented in the centrifuge with their symmetry axis parallel to the gyration radius. Thus, the axial z-coordinate of the samples is parallel to the direction of the centrifuge acceleration. After centrifuging, the samples were cut along the vertical axis and polished sections were prepared. To verify, to what extent the Fe–S melt segregated through the silicate matrix, and to evaluate the amount of silicate melt present, an image analysis has been carried out on backscattered electron (BSE) pictures of the experimental run products. BSE images (Fig. 1a–d) of 200×300 µm or 100×150 µm at points representing an x–y grid with steps of 100 µm were taken with an electron microprobe JEOL JXA 8200. Each image was analyzed with the digital image tool software 'DIAna Image Analysis' to determine the silicate and Fe–S melt proportions. Then, maps of silicate and Fe–S melt distributions have been constructed (Figs. 2–4), and average silicate and Fe–S melt fraction profiles have been determined along the centrifuge acceleration parallel z-coordinate of the cylindrical samples (Fig. 5), excluding the outer 100 µm at the vertical borders of each capsule.

4. Results

4.1. Melt segregation

Three static and nine centrifuging experiments have been performed (Table 1) mainly varying metal and silicate melt proportions through variations in bulk composition and temperature, respectively. In all centrifuged samples, the segregation of the Fe–S and silicate melts has been observed. The segregation of Fe–S melt is always in the direction of the gravity acceleration and the segregation of silicate melt is in the opposite, gravitationally upward direction, as to be expected from the density contrasts. The first two experiments have

Table 1
Conditions and results of experimental runs.

Run	Composition	$Fe_{70}S_{30}$[a] (vol.%)	T (°C)	Static time (h)	Acceleration (g)	Centrifuge time (h)	Sample[b] height (mm)	Silicate melt (vol.%)		Fe–S (vol.%)	
								Top	Bottom	Top	Bottom
Sample1	Peridotite[c] + $Fe_{70}S_{30}$	5.0	1215	72	1	–	2.00	7.6	7.4	7.5	7.6
Sample2	Peridotite[c] + $Fe_{70}S_{30}$	5.0	1255	70	500	2	2.30	12.8	7.6	5.2	4.7
Sample3	Peridotite + $Fe_{70}S_{30}$	5.0	1215	64	500	10	2.41	14.3	10.3	4.2	6.6
Sample4	Peridotite	0	1260	78	500	10	2.10	20.2	14.3	–	–
Sample5	Peridotite + $Fe_{70}S_{30}$	29.5	1150	90	600	8.5	2.14	16	7.5	11.0	17.0
Sample6	Peridotite + $Fe_{70}S_{30}$	15.1	1215	68	500	10	2.44	12.2	2.4	10.0	18.5
Sample7	Peridotite + $Fe_{70}S_{30}$	15.1	1150	76	500	10	2.32	–	–	13.4	16.1
Sample8	Peridotite + $Fe_{70}S_{30}$	4.3	1150	92	500	10	2.38	–	–	4.2	5.4
Sample9	Peridotite + $Fe_{70}S_{30}$	29.5	1280	88	1	–	2.22	29.0	22.0	7.5	30.5
Sample10	Peridotite + $Fe_{70}S_{30}$	29.5	1280	71	700	7	2.20	24.1	13.1	8.8	13.8
Sample11	Peridotite + $Fe_{70}S_{30}$	4.3	1280	80	700	8.5	1.95	17.0	14.8	2.2	2.6
Sample12	Peridotite + $Fe_{70}S_{30}$	29.5	1150	78	1	–	2.25	–	–	30.0	29.5

The calculated average content of melt does not always correspond to the mean values between the top and bottom melt fraction due to non-linear distribution of melt.
[a] Corresponds to the initially loaded quantity of $Fe_{70}S_{30}$.
[b] Sample height refers to the length of the cylindrical sample along its axis which is parallel to the gravity vector and corresponds to the z-direction.
[c] Grain size 60–120 µm, all other samples: grain size ~20–30 µm.

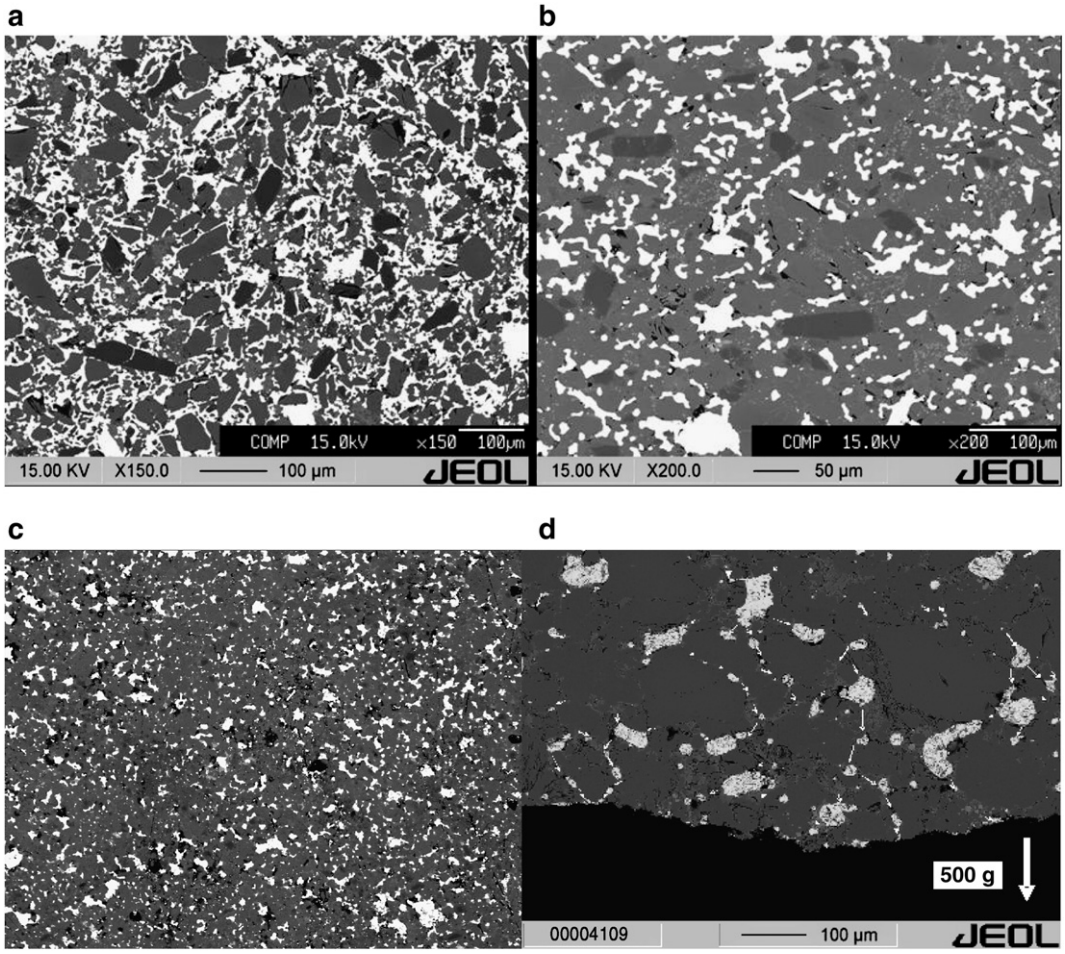

Fig. 1. a–d: BSE image of run products. Centrifuge acceleration is downward. White colour is FeS, dark grey colour is orthopyroxene, grey colour is olivine, and light grey colour is recrystallized spinel. (a) and (b): Peridotite samples with initially ~29.5 vol.% Fe–S. Under dynamic conditions the connectivity of Fe–S melt is much less than in a statically annealed sample. (a): Sample 12, statically annealed at T_{max} = 1150 °C for 78 h, with 30.2 vol.% FeS (no centrifuging). (b): Sample 5, annealed at 1150 °C for 90 h and centrifuged during 8.5 h at 600*g*. (c): Sample 7, peridotite with ~15.1 vol.% of Fe–S melt, but without silicate melt after 10 h of centrifuging at 1150 °C and 500*g*. The width of the image is ~2 mm, compare to Fig. 4b. (d): Sample 2, partially molten peridotite with 5 vol.% of Fe–S and 10.8 vol.% silicate melt after 2 h of centrifuging at 1255 °C and 500*g*. The arrows show the path of percolation of metal melt to the lower boundary of the sample. These paths coincide with the large melt pools near grain boundaries. The mechanism of flow can be represented as a creep of small droplets in channels filled with silicate melt. The black lower part corresponds to the graphite capsule. In this image, the dark grey colour is the peridotite matrix and the light grey colour is the silicate melt. The large white arrow shows the direction of the accelerative force.

been run with relatively coarse grained peridotite powders (60–120 μm). To improve textural maturation, all further experiments have been run with finer grained material (20 μm). The first experiment, sample 1 (Table 1), which was not centrifuged after annealing at 1215 °C in a static piston cylinder has been used as a reference of the vertical static silicate and Fe–S melt distribution. With the moderate

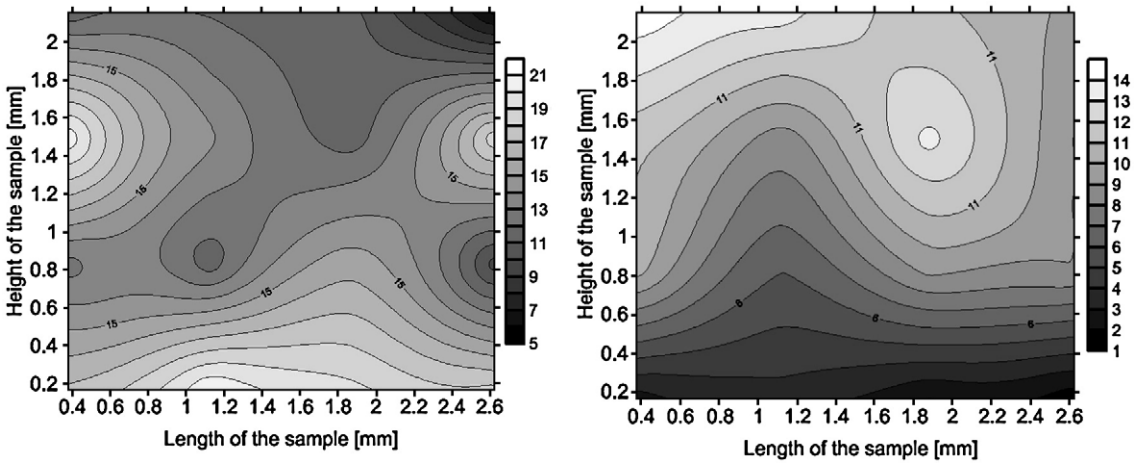

Fig. 2. Distribution of Fe–S liquid (left panel) and silicate melt (right panel) after 10 h of centrifuging at 1215 °C and 500*g* (sample 6). The average Fe–S melt content is 14.4 vol.% (~30 wtvol.%), the average silicate melt content is 8.6vol.%.

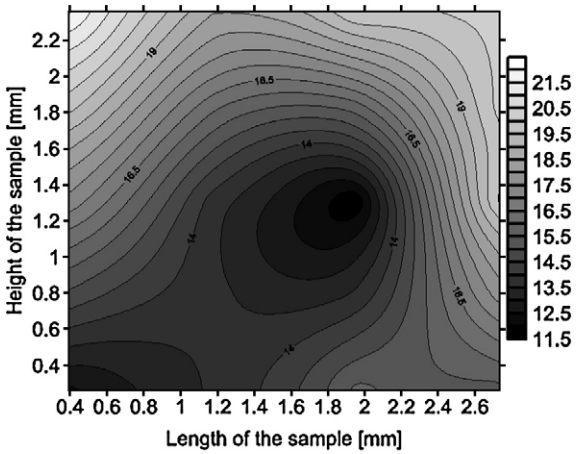

Fig. 3. Distribution of silicate melt after 10 h of centrifuging at 1260 °C and 500*g* (sample 4). The average silicate melt content is 16.6 vol.%., this sample does not contain Fe–S.

silicate melt fraction of 7.5 vol.% (Table 2), both the silicate and the metal melt (7.4 vol.% observed, Table 2) distribution were found to be homogeneous within the error of measurement. A second static experiment (sample 12, Fig. 1a) with initially 29.5 vol.% Fe–S was run at 1150 °C, i.e. below the silicate solidus. Even with this large amount of the Fe–S melt, the segregation of the metal was not observed. A third static experiment (sample 9), also with initially 29.5 vol.% Fe–S, was then run at 1280 °C, which led to a 26 vol.% silicate melt. With this silicate melt fraction, the segregation of silicate and metal melt has been observed even at 1*g* (Table 2).

Fig. 1a and b demonstrates the effect of static (sample 12, Table 1) and dynamic centrifuge assisted annealing (sample 5, Table 1) in a sample with initially 29.5 vol.% of the Fe–S melt. The statically annealed sample exhibits a perfectly developed network of the Fe–S melt. After centrifuging, the connectivity of melt decreased due to movement of the Fe–S melt which leads to a partial separation of the Fe–S melt from the matrix during centrifuging. In total, six experiments with silicate melt fractions between 9 and 20 vol.% and Fe–S melt fractions of 4–30 vol.% have been centrifuged at 500–700*g*. In all of these, silicate and metal melt segregation has been observed (Figs. 2–4) and quantified (Tables 1 and 2).

Sample 4 (Table 1) was run without a metal fraction, and an upward segregation of silicate melt (16.6 vol.%) is observed after centrifuging (Fig. 3). Sample 5 was intended as containing metal melt but no silicate melt and has been annealed at 1150 °C well below the melting point of fertile peridotite at c. 1200 °C at 1 GPa (Walter, 2003). Nevertheless, this sample contains 12.7 vol.% of the silicate melt. This could be due either to a lowering of the solidus through Fe^{2+} contamination of the peridotite stemming from the high content of the Fe–S melt (29.5 vol.%) or an incorrectly placed thermocouple. It can also be due to some of the Fe–S melt that left the graphite capsule and contaminated the thermocouple so that the indicated temperature was lower than the true one. Whatever the reason, our primary variable is a silicate melt fraction, which is observed after the experiment. A second experiment annealed and spun at temperatures below the melting point of the silicate matrix was thus conducted (sample 7, Fig. 1c). In this experiment the segregation of the Fe–S melt still occurs (Fig. 4b), but is one order of magnitude slower than in samples with comparable Fe–S melt contents but with the silicate melt present.

For most centrifuged samples, we observe a steady gradient $d\varphi/dz$, however, sample 6 containing 8.6 vol.% of silicate melt, has higher segregation rates in the upper and lower part of the capsule, as e.g. compared to sample 7 (Fig. 5).

4.2. Segregation velocity and permeabilities

Using Eq. (4), the segregation velocities of the silicate and Fe–S melts have been calculated from their distributions along the *z*-coordinate of the capsules (Table 2). Instead of 1*g*, the appropriate centrifugal acceleration of 500–700*g* has been used in Eq. (4). In the presence of a silicate melt, the Fe–S melt flows in the form of droplets from one triple junction to the adjacent one in channels filled with a silicate melt (Fig. 1d). For such experiments, the vertical contrast of the Fe–S distribution develops faster than in those without a silicate melt. In one experiment (sample 11, Table 1) at 1280 °C, the gyration time 8.5 h, and 700*g* acceleration, the silicate melt segregated from the initial c. 20 vol.% to 16 vol.% and all but 2.2–2.7 vol.% of the Fe–S melt separated. This seems to be the lowest limit of the Fe–S concentration left in the silicate matrix after the segregation in the presence of a silicate melt. In most samples the starting vol.% of Fe–S was observed as an average Fe–S vol.% after the centrifuging. Nevertheless, for samples 5 and 10 the discrepancy between the starting Fe–S fraction and the post-experiment Fe–S fraction largely exceeded the error of

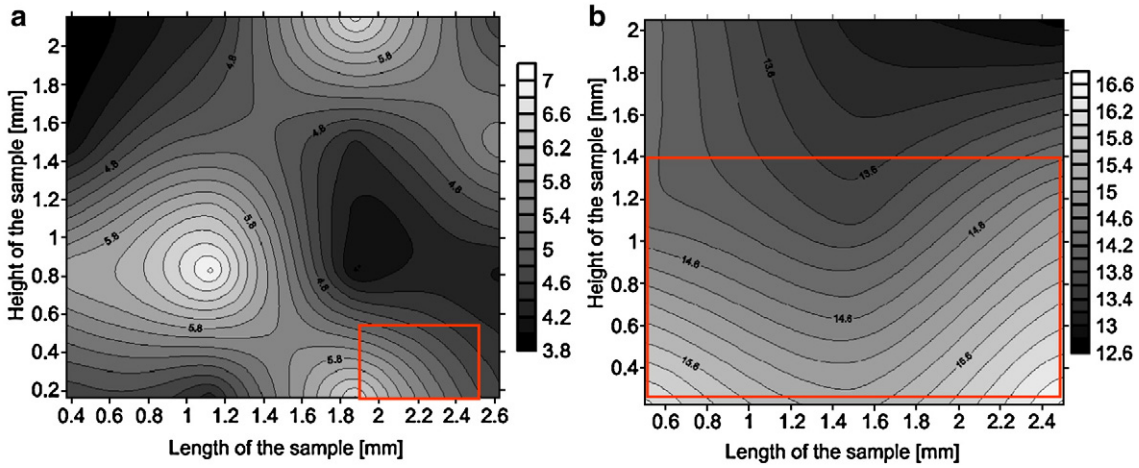

Fig. 4. Distribution of Fe–S liquid after centrifuging. (a) Sample 2, after 2 h of centrifuging at 500*g*, 1255 °C, initial Fe–S melt content of 5 vol.% (~10 wtvol.%. The marked square corresponds to the image in Fig. 1d. (b) Sample 7, after 10 h of centrifuging at 500*g* and 1150 °C, the initial and measured average Fe–S melt content are 15.1 and 14.6 vol.% (~30 wt. %). The capsule height is 2.28 mm. The marked square corresponds to the image in Fig. 1c. This sample does not contain silicate melt as run at conditions below the peridotite solidus.

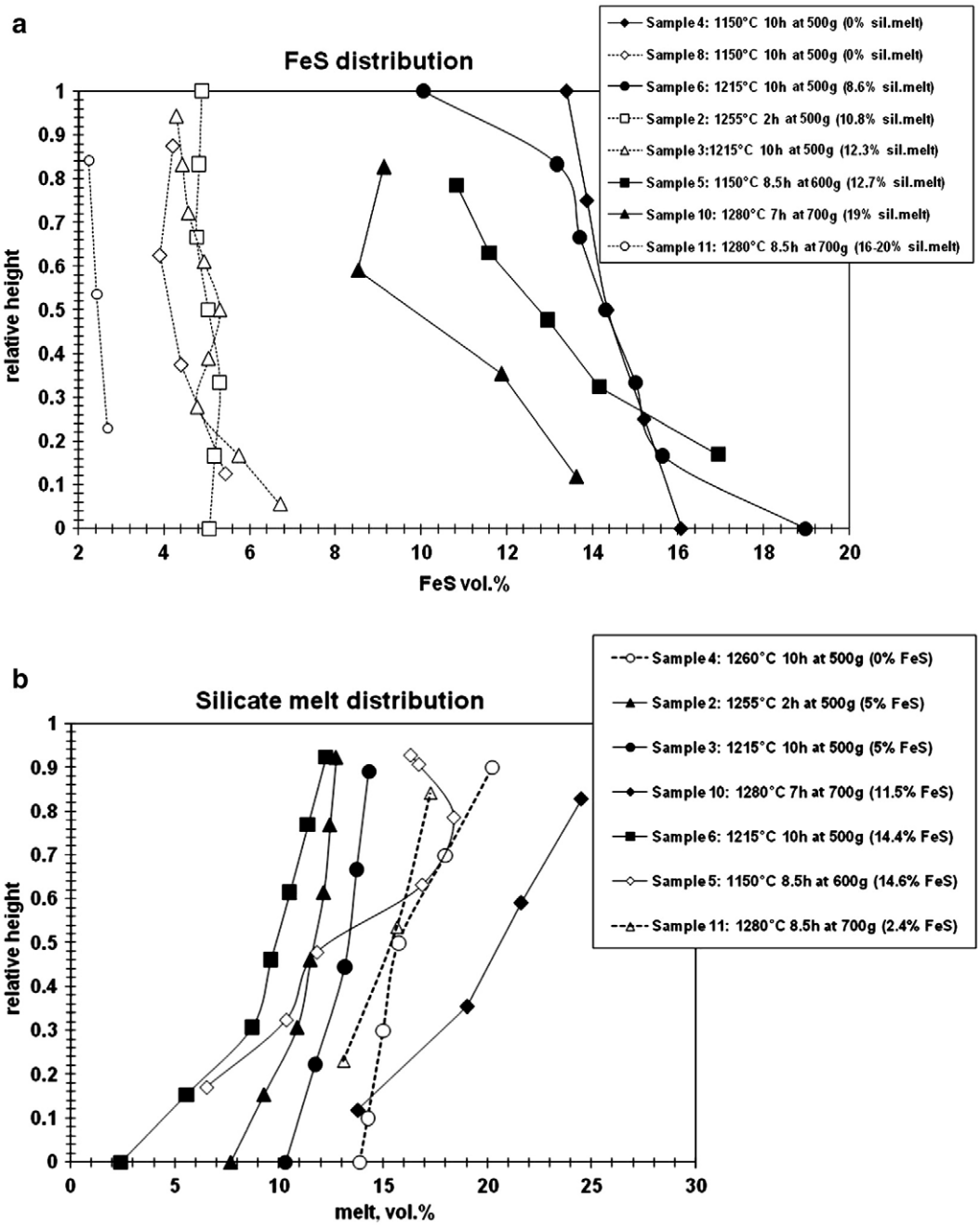

Fig. 5. Results of the image analysis of centrifuged samples. The average contents of silicate and Fe–S melt are given in brackets. (a) *Upper panel:* Fe–S melt distribution along the capsule height. The height is normalized to the length of capsules. In the calculation of the segregation velocity the mean value of the vertical gradient of Fe–S was taken into account. Samples with lower content of Fe–S demonstrate smaller gradients of Fe–S concentration and lower percolation rates. (b) *Lower panel:* Silicate melt distribution in partially molten peridotite samples.

measurement. In these two samples, 16 and 18 vol.% of the Fe–S melt escaped from the gravitational bottom of the capsules, as the graphite capsules do not provide a complete conservation of the Fe–S melt. For the calculation of the Fe–S melt migration rate in these two samples (i.e. 5 and 10), the initial vol.% of Fe–S from Table 1 was used in Eq. (4), and $\Delta\varphi$ has been taken as a difference between the observed vol.% of Fe–S and the initial one, yielding a minimum Fe–S melt percolation rate.

Segregation velocities v_f of the metal and silicate melt were calculated according to Eq. (3) (Table 2, Fig. 6). For the centrifuged samples, the melt migration velocities relative to the barycentre and normalized to 1 g are between 7.6×10^{-5} and 5.8×10^{-4} mm/h for the silicate melt, and -4.2×10^{-5} to -2.8×10^{-4} mm/h for the metal melt, both depending on the melt fractions present.

Using the relationship between Darcy's flow velocity and permeability (McKenzie, 1984), we also calculated the permeability κ of the solid matrix (Table 2)

$$\kappa = \frac{\varphi}{1-\varphi}\cdot\frac{\eta\cdot v_f}{\Delta\rho\cdot g} \tag{5}$$

in samples which underwent a two phase flow, i.e. either contains only the Fe–S melt or only the silicate melt. In Eq. (5), φ is the porosity or melt fraction, η the shear viscosity of the melt, v_f the melt percolation velocity, and $\Delta\rho\cdot g$ the pressure gradient. The employed melt viscosities are 0.1 Pa s for the silicate melt (Liebske et al., 2005), and 0.01 Pa s for the Fe–S melt (Alfè and Gillan, 1998; Urakawa et al., 2001). Sample 4 with 16.6 vol.% of partial silicate melt yields a

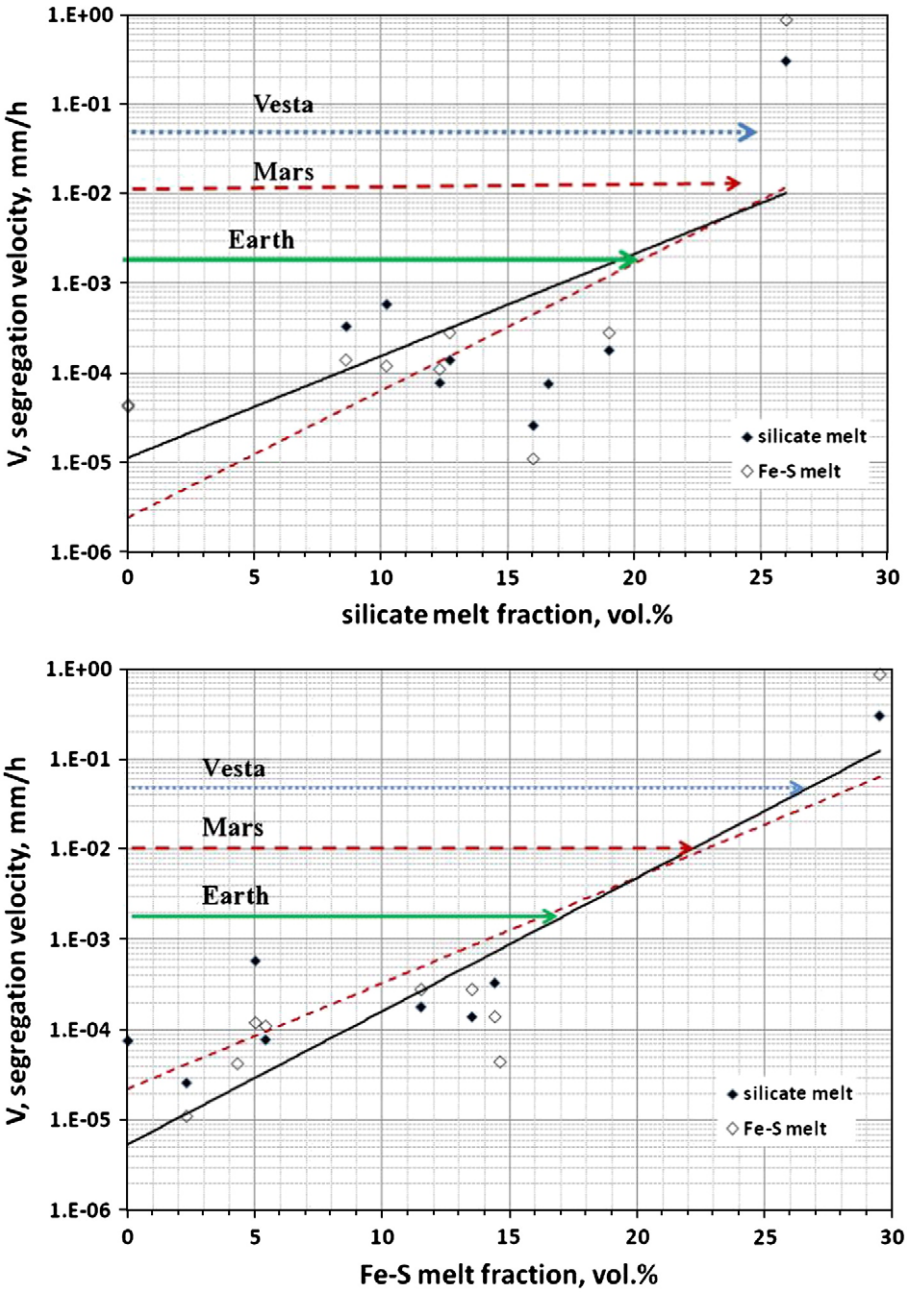

Fig. 6. Measured segregation velocities of silicate melt and Fe–S melt in fertile peridotite (data from Table 2). Upper panel: The scarce data of the segregation velocity as a function of silicate melt content are attributed to the differing content of Fe–S melt in samples. Dashed line stands for the correlation of silicate melt segregation velocity vs silicate melt fraction ϕ: $V_{\text{silicate melt}}(\text{mm/h}) = 2\cdot 10^{-6}\cdot e^{0.33\cdot\phi}$. Solid line represents the correlation between segregation velocity of Fe–S and silicate melt fraction: $V_{\text{Fe–S}}(\text{mm/h}) = 10^{-5}\cdot e^{0.26\cdot\phi}$. Lower panel: The correlation between segregation velocity and Fe–S content is more obvious. Dashed line stands for the correlation of silicate melt segregation velocity vs Fe–S melt fraction ϕ: $V_{\text{silicate melt}}(\text{mm/h}) = 2\cdot 10^{-5}\cdot e^{0.27\cdot\phi}$. Solid line represents the correlation between segregation velocity of Fe–S and silicate melt fraction: $V_{\text{Fe–S}}(\text{mm/h}) = 5\cdot 10^{-6}\cdot e^{0.34\cdot\phi}$. Horizontal arrows indicate a typical migration velocity of Fe–S in order to form metallic core by percolation process. Segregation velocities for Vesta and Mars are reduced to the Earths conditions.

permeability of 8.5×10^{-17} m². Samples containing 4.3 and 14.6 vol.% of Fe–S (samples 7 and 8) possess calculated permeabilities of 1.2×10^{-18} m² and 2.8×10^{-19} m², respectively. The latter permeabilities are 2–3 orders of magnitude lower than those reported by Roberts et al. (2007).

5. Discussion

5.1. The role of silicate melt for the segregation of Fe–S melts

Our experiments (Table 2, Fig. 6) suggest that the Fe–S segregation velocity strongly depends on the silicate and Fe–S melt fractions, nevertheless, Fe–S segregation velocities could also correlate with the silicate matrix viscosity. We thus corrected the diffusion creep viscosity $\eta_0 = 10^{14}$ Pa s of peridotite (at 1150 °C and 20 μm grain size, Zimmerman and Kohlstedt, 2004; Scott and Kohlstedt, 2006) for melt fraction and temperature according to

$$\eta = \eta_0 \cdot \exp(-21\cdot\varphi)\cdot \exp\left[-\frac{Q}{R}\left(\frac{1}{1423}-\frac{1}{T}\right)\right], \quad (6)$$

where Q is 370 kJ/mol, R the universal gas constant, and T temperature in K (Zimmerman and Kohlstedt, 2004). The relative viscosity $\eta(\varphi\ T)/\eta_0$ is given in Table 2, any correlation with segregation velocities is

Table 2
Calculated migration velocities and permeabilities of Fe–S and silicate melts in peridotite.

Run name	Silicate melt (%)	Metal melt (%)	$V_{segr.\ Silicate}$[a] (mm/h)	$V_{segr.\ Metal}$[a] (mm/h)	Permeability (m^2)	Viscosity factor[b]
Sample 1	7.5	7.4	–[c]	–[c]	–	–
Sample 2	10.2	5.0	5.8×10^{-4}	-1.2×10^{-4}	–	0.014/0.05
Sample 3	12.3	5.4	7.8×10^{-5}	-1.1×10^{-4}	–	0.019/0.06
Sample 4	16.6	0	7.6×10^{-5}	0	8.6×10^{-17}[d]	0.003
Sample 5	12.7	13.5[e]	1.4×10^{-4}	-2.8×10^{-4}[e]	–	0.085/0.004
Sample 6	8.6	14.4	3.3×10^{-4}	-1.4×10^{-4}	–	0.055/0.003
Sample 7	0	14.6	–	-4.4×10^{-5}	1.1×10^{-18}[f]	1/0.045
Sample 8	0	4.3	–	-4.2×10^{-5}	2.8×10^{-19}[f]	1/0.37
Sample 9	26	29.5	0.30	−0.87	–	$3\times10^{-4}/6\times10^{-6}$
Sample 10	19	11.5[e]	1.8×10^{-4}	-2.8×10^{-4}[e]	–	$1.5\times10^{-3}/10^{-4}$
Sample 11	16[g]	2.4[h]	2.6×10^{-5}	-1.1×10^{-5}	–	$10^{-3}/1.2\times10^{-3}$
Sample 12	0	30.2	–[c]	–[c]	–	–

[a] Migration velocity is calculated for 1 *g*.
[b] Two numbers separated by slash are estimations assuming matrix porosity to be equal to the silicate melt fraction and matrix porosity to be equal to silicate melt + FeS fraction.
[c] Static experiments, which did not result in any melt segregation.
[d] Calculated from Eq. (4) permeability employing a silicate melt viscosity of 0.1 Pa s (Liebske et al., 2005). The density contrast between silicate melt and solid peridotite matrix is assumed as 0.5×10^3 kg/m³ (McKenzie, 1989).
[e] In these experiments with initially 29.5 vol.% of Fe–S, the metal melt accumulated at the bottom of the capsule and partially left the graphite capsule, here the fraction of melt is reported which remained in the peridotite matrix after centrifuging. The calculated segregation velocities of the metal melt is based on the observed $\Delta\varphi$ in the silicate matrix and represents the segregation velocity at the observed melt fraction while segregation velocities for the completely segregated melt fractions were significantly higher.
[f] For calculation of permeability the Fe–S viscosity is taken as 0.01 Pa s (Alfè and Gillan, 1998; Urakawa et al., 2001). The density contrast between Fe–S melt and solid peridotite matrix is taken as 1.9×10^3 kg/m^3 (Secco et al., 2002).
[g] In this experiment some silicate melt escaped and collected at the upper boundary of the capsule. The silicate melt migration rate is calculated assuming an initially homogeneously distributed melt fraction of 20 vol.%.
[h] The initial content of FeS was 4.3 vol.%, some of the FeS was found in the bottom layer of the capsule.

absent and we thus conclude that segregation velocities mainly depend on the melt fractions present.

In the absence of the silicate melt, the percolation velocity of the Fe–S melt between 4 and 14 vol.% of Fe–S is slow and practically constant (Table 2). In this volume fraction range, a slow segregation was proposed to occur because of the sinking of individual droplets of the metallic melt (Yoshino and Watson, 2005). However, the segregation of the Fe–S melt cannot be simulated with the simple Stokes sinking velocity of Fe–S melt droplets in the peridotite matrix. For bulk viscosities of 10^{14} Pa s for unmolten peridotite at 1150 °C (Zimmerman and Kohlstedt, 2004) and of 8×10^{12} to 3×10^{10} Pa s for melt fraction and temperature corrected partially molten peridotite (Eq. (6)), a density contrast of 1.9×10^3 kg/m^3, and a maximum size of 10 μm for the largest Fe–S melt inclusions, estimations of Stokes velocities are from 10^{-14} to 10^{-11} mm/h. These Stokes velocities are 7–9 orders of magnitude slower than those experimentally observed during the centrifugation (Table 2). Thus, in unmolten and in partially molten peridotite, the Fe–S melt segregates very slowly through a percolation flow. The question remains whether this Fe–S melt network is continuous or discontinuous.

Above the volume fraction of 14–15 vol.% of the Fe–S melt, the amount of silicate melt is not critical for the segregation rate of the metallic phase, as experimentally demonstrated through the comparison of samples 5, 6 and 7. Furthermore, sample 9 with 29.5 vol.% of the Fe–S melt segregated very rapidly to an average metal melt fraction of 14–15 vol.% after annealing over 88 h at 1 *g*, i.e. without centrifuging. This sample contained 26 vol.% of the silicate melt, thus, the segregation of Fe–S and the silicate melt was efficient even at a normal gravity. Sample 10 is a repetition of sample 9, but has been centrifuged at 700 *g* during 7 h. The amount of the silicate melt in this sample (19 vol.%) is smaller than in sample 9 (26 vol.%), and 18 vol.% Fe–S have been centrifuged completely out of the silicate matrix, leaving 8.8 (top) to 13.8 vol.% (bottom) Fe–S melt. Similar, sample 5 had 16 vol.% Fe–S melt centrifuged out of the sample, leaving 11.0 (top) to 17.0 vol.% (bottom) Fe–S melt (Table 1). This is interpreted as a fast segregation until reaching a metal melt volume fraction of about 15%, and then, the segregation of Fe–S melt is slowed down. We deduce a percolation limit of a permeable flow for Fe–S melt in partially molten peridotite around 15 vol.% of Fe–S. Below 15 vol.% Fe–S, linear gradients of the Fe–S distribution are always observed in all centrifuged samples (Fig. 5).

The comparison of silicate and Fe–S migration rates (Table 2) demonstrates that the flow velocities of the two liquid phases are correlated. The segregation flow of the Fe–S melt increases with the migration rate of silicate melt, and vice versa. This suggests that not only the metal or silicate melt fraction but also the total porosity of the peridotite matrix control the rates of melt segregation.

Beside the 15 vol.% threshold of a fast percolation for the metal melt, a second, lower threshold of the Fe–S melt segregation is 2.0–2.5 vol.%. A redistribution of Fe–S below this fraction was not observed, instead, the centrifuge experiments demonstrate an almost constant Fe–S volume fraction of 2.2–2.7 vol.%, even after several hours of centrifuging at 700 *g* (sample 11, Fig. 5). Thus, it is practically impossible to remove the Fe–S melt below 2 vol.% from a peridotite matrix until the matrix is molten to ≥25 vol.%. At such higher degrees of melting, the gravitational segregation of olivine crystals could occur in a form of a hindered sedimentation and the mechanism of the Fe–S flow will then change from a percolation to a suspension flow type.

The centrifuging experiments have demonstrated a considerable but still slow percolation of Fe–S melts under an increased acceleration of 500–700 *g*. The slow percolation of Fe–S melts in olivine-basalt aggregates has also been demonstrated in a temperature gradient field (Holzheid et al., 2000). The calculated percolation and melt flow velocities of Fe–S are different in the presence and absence of the silicate melt. In the solid peridotite assemblage, the calculated percolation velocity is one order of magnitude smaller than in samples with 14–15 vol.% of the silicate melt, the presence of the silicate melt facilitating the segregation of Fe–S melts. Channels filled with the silicate melt are well interconnected and the silicate melt flow is realized through an interconnected network.

5.2. Permeabilities

The permeabilities calculated from the measured segregation velocity for Fe–S melt in the centrifuge experiments are 1.2×10^{-18} to 2.8×10^{-19} m² for porosities of 4.3 and 14.6% and grain sizes of 20–30 μm. This is comparable to 2×10^{-15} m^2 for a porosity of 10% and a grain size of 45 μm as calculated from the melt geometry of the static

Fe–S distribution in unmolten olivine aggregates by Roberts et al. (2007). When scaled to the grain size, our effective permeability is 2 orders of magnitude lower than the theoretically derived from Roberts et al. (2007). A possible explanation may be that the calculated permeability from a static distribution of pores as done by Roberts et al. (2007) is only a hydraulically constrained parameter obtained from a frozen pattern of the melt distribution. Such an estimation does not take into account rheological effects of sliding and dynamic rearrangement of grains and melt during the porous flow of Fe–S accompanied by local rearrangements of mineral grains. Secondly, the short annealing times of the coarse grained olivine aggregates of Roberts et al. (2007) might not have produced a steady state Fe–S melt distribution. Roberts et al. (2007) underline, that their annealing time of 24 h for an average grain size of 45 μm is sufficient to obtain equilibrium dihedral angles, however, Faul (1997) on olivine–silicate melt pointed out, that, although dihedral angles remain constant, the melt distribution is transient unless run times of 2–3 weeks are achieved. Alternatively, the assumption that during experiments the compaction of the solid matrix was negligible is not fully correct. If the lower boundary of samples was impermeable, than the scaling factor $\sim\delta_c/h$ appears in the right-hand side of Eq. (5) and the estimated permeabilities would be 2–3 orders of magnitude higher.

This study will not resolve this discrepancy; nevertheless, the centrifuge experiments determine an effective permeability of the peridotite matrix for the Fe–S melt. Further, we directly employ the measured segregation velocities and do not involve calculated permeabilities for estimating the time scales of core segregation through a percolative flow in a partially molten silicate mantle. The employment of measured v_f for the migration problem of Fe–S and silicate melts in the mantle is justified because in the mantle the travelled distance $z \gg \delta_c$, and in this case the migration velocity is $\sim v_o$ (McKenzie, 1984).

5.3. Core formation mechanism and time scale

According to the present study and to Yoshino and Watson (2005), the presence of a silicate melt leads to coarsening of the Fe–S melt pools which in turn may decrease the segregation velocity for molten Fe–S. At higher contents of silicate melt, the local coagulation of Fe–S droplets is faster and the size of Fe–S droplets increases. Extrapolation of the minimum amount of silicate melt to provide a segregation velocity (for Fe–S) fast enough to complete core formation in a plausible time (i.e. ≤100 Ma on Earth), indicates that the silicate melt fraction could be even larger than the limit for "Rayleigh–Taylor" instabilities of 20–25 vol.%, a limit of the dense suspension (Stevenson, 1990), in a partially molten aggregate.

The question remains what is the percolation velocity of the peridotite matrix which on the one hand satisfies the core formation time and on the other provides nearly complete separation of Fe–Ni–S melts into the core with a residual fraction of ~1 vol.% of Fe–Ni–S stranded in the Earth's mantle (Jones and Drake, 1986). The purely mechanical percolation process of Fe–S melts (without the pressure-solution of crystals in the presence of silicate melts) cannot provide a core formation mechanism due to a high permeability threshold of Fe–S–melt in mantle silicates. The percolation threshold of 2–3 vol.% for Fe–S in a silicate matrix is not compatible with the present sulphur concentration in the mantle, which is <300 ppm (Jones and Drake, 1986). Natural findings in olivine-bearing rocks which contained a sulphide melt give evidence of a trapped sulphide fraction of 1.4–2.6 vol.% (Barnes et al., 2008), in accordance with our lower percolation threshold. Table 3 represents the parameters for the calculation of minimum segregation velocities of Fe–S in a peridotite reduced to conditions on Vesta, Mars and the Earth. Core formation times for the Earth can be roughly estimated by calculating the time needed for the metallic melt to percolate a half of a distance from 0 to 2900 km at a constant migration rate, as g is almost constant throughout the silicate mantle. To almost complete core formation within 80–90 Ma, a minimum percolation velocity of about 20 km/Ma, or $\sim 2\times10^{-3}$ mm/h (Fig. 6) is needed. Within a partially molten peridotite, this may be achieved only at a partial silicate melting >20–25 vol.% and the Fe–S contents above the fast percolation threshold (>14 vol.%). Only in this case, core formation times due to the percolation are close to the estimations of Allègre et al. (1995, 2008) and Halliday (2008).

Table 3
Estimated core formation velocities on Vesta, Mars and Earth.

Object	Vesta	Mars	Earth
Mean radius [km]	270	3390	6371
Radius core [km]	123	1900	3485
g [m/s^2]	0.28	3.71	9.81
Silicate mantle thickness [km]	147	1490	2886
Hf/W age (single stage) [Ma][a]	2.0–4.6	1–10	12–33
Assumed core formation time [Ma]	3	10	85[b]
Average velocity of Fe–S migration (scaled Earth's gravity[c]) [mm/h]	5.2×10^{-2}	1.1×10^{-2}	1.9×10^{-3}

[a] Kleine et al. (2002).
[b] See discussion in Allègre et al. (2008).
[c] Core formation velocities are estimated from a half of the actual planetary mantle thicknesses and the assumed core formation time. To reduce Fe–S velocities to the Earth's conditions density contrast is assumed as follows: for the Earth $\Delta\rho_{Fe-S} = 1.9\times10^3$ kg/m^3 and $g=1$, for Mars and Vesta $\Delta\rho_{Fe-S} = 4\times10^3$ kg/m^3 and $g=0.38$ and $g=0.0255$, respectively (Bertka and Fei, 1997; Ghosh and McSween, 1998).

For smaller planetary objects such as Vesta, the time scale of a complete metallic core formation in the case of the Fe–S percolation flow would be unrealistically large for the measured segregation velocities around 10^{-4} mm/h (Table 2 and Fig. 6). To satisfy an estimated core formation time of 3 Ma (Kleine et al., 2002), even faster segregation velocities than on the Earth would be required: Scaled to the Earth's g and density contrast, a percolation velocity of 5×10^{-2} mm/h would be needed on Vesta. Compared to the Earth, the segregation distance decreases for smaller planetesimals, but as the gravitational constant decreases over-proportionally, the driving force for gravitational segregation becomes less and thus the segregation gets more difficult. One possibility to overcome the slow segregation rates would be, if the experimental conditions were too reduced to apply to this small planetary body. As shown by Terasaki et al. (2008) the wetting angle of the Fe–S melt could be less than 60° for oxidizing conditions and smaller Mg# of silicates, and thus the interconnection of the Fe–S melt phase could become possible, providing much shorter core segregation times.

It is similarly difficult to reconcile the core formation time for Mars-sized planetary embryos, which accrete within <10 Ma (Chambers, 2004), with the percolation velocity observed in the experiments (Fig. 6). This indicates that percolation cannot be the dominant core formation mechanism in terrestrial planets.

Nevertheless, high silicate melt fractions, as needed to make percolation viable, are possible during accretion when impacts become energetic enough to lead to a significant melting on planetary embryos. This point is reached at latest when the accreting planets reach the Mars mass (Melosh, 1990; Tonks and Melosh, 1992). Percolation therefore could contribute to transport of iron melt through partially molten peridotites. This stage will always occur when accreting planets begin to heat and the previously completely solid silicate fraction begins to melt. The core formation will thus be initiated through the percolation of the Fe–S melt through the partially molten silicate mantle and in particular any volume fraction above the percolation threshold of 14–15% could segregate through this mechanism. The percolation might also occur in the lower, only partially molten parts of magma ponds or within the marginal zones of magma oceans. There, the iron agglomerates to form the iron diapirs which then sink into the centre of the planet and form the iron core (Rubie et al., 2003; Walter and Tronnes, 2004).

From the present study three facts were established:

(1) For Fe–S fractions up to 15 vol.%, the percolation is not fast with or without silicate melt. Only at a threshold >15 vol.% this process could be responsible for an initial stage of core formation resulting in metal cores equal to a few percent of the planetesimals volume.
(2) The effective permeability of silicate melt in a peridotite is 10^{-16}–10^{-17} m^2 at 10–15 vol.% of a partial melting employing the silicate melt viscosity 0.1 Pa s.
(3) In a peridotite matrix without a partial silicate melting, the effective permeability of Fe–S liquids is 10^{-18}–10^{-19} m^2 at 5–15 vol.% Fe–S melt employing the viscosity of molten Fe–S of 0.01 Pa s. This is in contrast in comparison with the results from static annealing experiments, where the permeability of Fe–S melts without partial silicate melting has been estimated to 10^{-15} m^2 at 10 vol.% of Fe–S (Roberts et al., 2007), but it is in a full agreement with the conclusions of Walte et al. (2007) on the low mobility of a melt phase in a solid matrix with high wetting angles.

The transport of Fe–S liquids occurs via sinking of small droplets in channels already filled with a partial silicate melt. The sinking process is slow enough to equilibrate the Fe–S melt with the silicate melt. The Fe–S phase is not interconnected during the sinking process but still movable and raining through channels. Due to the counter flows of the buoyant silicate melt and sinking Fe–S droplets, the effective viscosity which dominates the viscous flow is the shear viscosity of the partial silicate melt. This may explain why the segregation of silicate and Fe–S melts occurs on the same time scale, regardless of the difference of their viscosities.

The experiments performed in this study confirm that either (i) a high degree of silicate melting on early formed planetesimals like Vesta is needed for a complete core segregation to take place (Stevenson, 1990; Taylor, 1992; Greenwood et al., 2005), a result confirmed numerically by Merk et al. (2002), or (ii) a high oxygen fugacity (Terasaki et al., 2008) is needed to allow the rapid metal–silicate segregation. A possible alternative, at least for some initial segregation, is given by high shear stresses and deformation of a subsolidus silicate matrix, which allows the Fe–S melt to migrate into cracks (Bruhn et al., 2000; Rushmer et al., 2005). However, this mechanism is feasible only for the short temperature interval between the Fe–S and silicate solidi, but could help to initiate segregation through locally increased Fe–S fractions.

6. Conclusions

In the light of the presented results on the percolation velocities of Fe–S melts in peridotite and partially molten peridotite, the segregation via a percolation flow could contribute to the formation of the core on the Earth, Mars and on planetesimals like Vesta only at the early accretion stage of the core segregation as suggested by Terasaki et al. (2008). The percolation flow of Fe–S alone is too slow to be the dominant core formation mechanism in terrestrial planets; it can nevertheless initiate core formation.

1. The segregation of Fe–S melt through the percolation in an unmolten olivine-dominated silicate matrix is too slow to contribute significantly to the core formation. Segregation within a partially molten silicate matrix is not fast enough to complete the core formation in Mars- and Earth-sized planetary bodies within a reasonable time, but may contribute considerably at the early accretion stage.
2. During the accretion of terrestrial planets, the percolation of Fe–S could have played some role in the upper parts of the silicate mantle during the period of giant impacts when the degree of the partial silicate melting was larger than 20–25 vol.%. Independent of the final core forming mechanism, the first significant Fe–S segregation may occur through the percolation of Fe–S melt droplets in a partially molten silicate matrix, as demonstrated in this study.
3. The lower percolation threshold for the "peridotite plus iron–sulphur" with partial silicate melt is 2–3 vol.%, and is almost compatible with the calculated "residual" amount of trapped sulphide melts in the Earth's mantle, which is around 1 vol.% (~2.0–2.5 wt.%, Jones and Drake, 1986), and with the experimental results of mechanical extraction of Fe–S melts under shear deformation ~1 vol.%, (Hustoft and Kohlstedt 2006).

Acknowledgements

We thank Jamie Connolly and Jim Mungall for thoughtful and very constructive suggestions, which helped to clarify the manuscript. GS was supported by ETH grant TH 20/03-2 and the centrifuge work by SNF grant 200020-111725-1.

References

Alfè, D., Gillan, M.J., 1998. First-principles simulations of liquid Fe–S under Earth's core conditions. Phys. Rev., B 58, 8248–8256.
Allègre, C.J., Manhès, G., Göpel, C., 1995. The age of the Earth. Geochim. Cosmochim. Acta 59, 1445–1456.
Allègre, C.J., Manhès, G., Göpel, C., 2008. The major differentiation of the Earth at ~4.45 Ga. Earth Planet. Sci. Lett. 267, 386–398. doi:10.1016/j.epsl.2007.11.056.
Bagdassarov, N., Dorfman, A., Dingwell, D.B., 1996a. Centrifuging of partially molten granites at high temperature: I. Compaction vs. deformation. Geophys. J. Int. 127, 616–626.
Bagdassarov, N., Dorfman, A., Dingwell, D.B., 1996b. Centrifuging of partially molten granites at high temperature: II. Rayleigh–Taylor instability and Stokes sedimentation. Geophys. J. Int. 127, 627–634.
Ballhaus, Ch., Ellis, D.J., 1996. Mobility of core melts during Earth's accretion. Earth Planet. Sci. Lett. 143, 137–145.
Barnes, S.J., Fiorentini, M.L., Austin, P., Gessner, K., Hough, R.M., Squelch, A.P., 2008. Three-dimensional morphology of magmatic sulfides sheds light on ore formation and sulphide melt migration. Geology 36, 655–658.
Bertka, C.M., Fei, Y., 1997. Mineralogy of the Martian interior up to core–mantle boundary pressures. J. Geophys. Res. 102, 5251–5264.
Boyet, M., Carlson, R.W., 2005. 142 *Nd* evidence for early (>4.53 Ga) global differentiation of the silicate Earth. Science 309, 576–581. doi:10.1126/science.1113634.
Brett, R., Bell, P.M., 1969. Melting relations in the Fe-rich portion of the system Fe–FeS at 30 kb pressure. Earth Planet. Sci. Lett. 6, 479–482.
Bruhn, D., Groebner, N., Kohlstedt, D.L., 2000. An interconnected network of core forming melts produced by shear deformation. Nature 403, 883–886.
Campbell, I.H., Roeder, P.L., Dixon, J.M., 1978. Plagioclase buoyancy in basaltic liquids as determined with a centrifuge furnace. Contrib. Mineral. Petrol. 67, 369–377.
Canup, R.M., Agnor, C.B., 2000. Accretion of the terrestrial planets and the Earth–Moon system. In: Canup, R.M., Righter, K. (Eds.), Origin of the Earth and Moon. Univ. of Arizona Press, pp. 113–129.
Chambers, J.E., 2004. Planetary accretion in the inner Solar System. Earth Planet. Sci. Lett. 223, 241–252. doi:10.1016/j.epsl.2004.04.031.
Faul, U.H., 1997. Permeability of partially molten upper mantle rocks from experiments and percolation theory. J. Geophys. Res. 102, 10299–10311.
Gaetani, G.A., Grove, T.L., 1999. Wetting of mantle olivine by sulphide melt: implication for Re/Os ratios in mantle peridotite and late-stage core formation. Earth Planet. Sci. Lett. 169, 147–163.
Ghosh, A., McSween, H.J., 1998. The thermal model for differentiation of asteroid 4 Vesta, based on the radiogenic heating. Icarus 134, 187–206.
Greenwood, R.C., Franchi, I.A., Jambon, A., Buchanan, P.C., 2005. Widespread magma oceans on asteroidal bodies in the early solar system. Nature 435, 916–918. doi:10.1038/nature03612.
Halliday, A.N., 2008. A young Moon-forming giant impact at 70–110 million years accompanied by late-stage mixing, core formation and degassing of the Earth. Philos. Trans. R. Soc., A 366, 4163–4181. doi:10.1098/rsta.2008.0209.
Hirschmann, M.M., Asimow, P.D., Giorso, M.S., Stolper, E.M., 1999. Calculations of peridotite partial melting from thermodynamic models of minerals and melts. III. Controls on isobaric melt production and the effect of water on melt production. J. Petrol. 40, 831–851.
Holzheid, A., Schmitz, M.D., Grove, T.L., 2000. Textural equilibria of iron sulfide liquids in partly molten silicate aggregates and their relevance to core formation scenarios. J. Geophys. Res. 105 (B6), 13,555–13,567.
Hustoft, J.W., Kohlstedt, D.L., 2006. Metal–silicate segregation in deforming dunitic rocks. Geochem. Geophys. Geosyst. 7, Q02001. doi:10.1029/2005GC001048.
Jones, J.H., Drake, M.J., 1986. Geochemical constraints on core formation in the Earth. Nature 322, 221–228.
Kadik, A.A., Lebedev, E.B., Dorfman, A.M., Bagdassarov, N.S., 1989. Simulating crystal–magma separation in a centrifuge. Geochem. Int. 26, 39–48.

Kadik, A.A., Dorfman, A.M., Bagdassarov, N.S., Lebedev, E.B., 1990. Influence of pyroxenes on the melt distribution in the intergranular space in peridotites. Geochem. Int. 27, 131–134.
Kleine, T., Münker, C., Mezger, K., Palme, H., 2002. Rapid accretion and early core formation on asteroids and the terrestrial planets from Hf–W chronometry. Nature 418, 952–955. doi:10.1038/nature00982.
Kleine, T., Mezger, K., Münker, C., Palme, H., Bischoff, A., 2004. ^{182}Hf–^{182}W isotope systematics of chondrites, eucrites, and Martian meteorites: chronology of core formation and early mantle differentiation in Vesta and Mars. Geochim. Cosmochim. Acta 68, 2935–2946. doi:10.1016/j.gca.2004.01.009.
Kleine, T., Palme, H., Mezger, K., Halliday, A.N., 2005. Hf–W chronometry of lunar metals and the age and early differentiation of the Moon. Science 310, 1671–1674. doi:10.1126/science.1118842.
Kopylova, M.G., Russell, J.K., 2000. Chemical stratification of cratonic lithosphere: constraints from Northern Slave Craton, Canada. Earth Planet. Sci. Lett. 181, 71–87.
Lebedev, E.B., Kadik, A.A., Kuskov, O.L., Dorfman, A.M., Lukanin, O.A., 1999. The motion of sulfide phases in a partially molten silicate material: application to the problem of the formation of planetary cores. Sol. Syst. Res. 33 (5), 346–350.
Lee, J., Agee, C.B., 1996. Geochemistry of mantle–core differentiation at high pressure. Nature 381, 686–689.
Li, J., Fei, Y., 2004. Experimental Constraints on Core Composition. Treatise of Geochemistry, vol. 2. Elsevier, New York, pp. 521–546.
Liebske, C., Schmickler, B., Tersaki, H., Poe, B.T., Suzuki, A., Funakoshi, K.-i., Ando, R., Rubie, D.C., 2005. Viscosity of peridotite liquid up to 13 GPa: implications for magma ocean viscosities. Earth Planet. Sci. Lett. 240, 589–604. doi:10.1016/j.epsl.2005.10.004.
Melosh, H.J., 1990. Giant impacts and the thermal state of the early Earth. In: Newsom, H.E., Jones, J.H. (Eds.), Origin of the Earth. Oxford Univ. Press, New York, pp. 69–83.
Merk, R., Breuer, D., Spohn, T., 2002. Numerical modeling of ^{26}Al-induced radioactive melting of asteroids considering accretion. Icarus 159, 183–191. doi:10.1006/icar.2002.6872.
McCammon, C., Kopylova, M.G., 2004. A redox profile of the Slave mantle and oxygen fugacity control in the cratonic mantle. Contrib. Mineral. Petrol. 148, 55–68. doi:10.1007/s00410-004-0583-1.
McKenzie, D., 1984. The generation and compaction of partially molten rock. J. Petrol. 25, 713–765.
McKenzie, D., 1989. Some remarks on the movement of small melt fractions in the mantle. Earth Planet. Sci. Lett. 95, 53–72.
Minarik, W.G., Ryerson, F.J., Watson, E.B., 1996. Textural entrapment of core-forming melts. Science 272, 530–533.
Mungall, J.E., Su, Sh., 2005. Interfacial tension between magmatic sulphide and silicate liquids: constraints on kinetics of sulphide liquation and sulphide migration through silicate rocks. Earth Planet. Sci. Lett. 234, 135–149. doi:10.1016/j.epsl.2005.02.035.
Nimmo, F., Agnor, C.B., 2006. Isotopic outcomes of N-body accretion simulation: constraints on equilibration processes during large impacts from Hf/W observations. Earth Planet. Sci. Lett. 243, 26–43.
Nimmo, F., Kleine, T., 2007. How rapidly did Mars accrete? Uncertainties in the Hf–W timing of core formation. Icarus 191, 497–504. doi:10.1016/j.icarus.2007.05.002.
Ricard, Y., Bercovici, D., Schubert, G., 2001. A two-phase model for compaction and damage. 2. Application to compaction, deformation, and the role of interfacial surface tension. J. Geophys. Res. 106, 8907–8924.
Roberts, J.J., Kinney, J.H., Siebert, J., Ryerson, F.J., 2007. Fe–Ni–S melt permeability in olivine: implication for planetary core formation. Geophys. Res. Lett. 34, L14306. doi:10.1029/2007GL030497.
Rubie, D.C., Melosh, H.J., Reid, J.E., Liebske, C., Righter, K., 2003. Mechanism of metal–silicate equilibration in the terrestrial magma ocean. Earth Planet. Sci. Lett. 205, 239–255.
Rushmer, T., Petford, N., Humayan, M., Campbell, A.J., 2005. Fe–liquid segregation in deforming planetesimals: coupling core-forming compositions with transport phenomena. Earth Planet. Sci. Lett. 239, 185–202.
Schmidt, M.W., Connolly, J.A.D., Günther, D., Bogaerts, M., 2006. Element partitioning: the role of melt structure and composition. Science 312, 1646–1650. doi:10.1126/science.1126690.
Scott, T., Kohlstedt, D.L., 2006. The effect of large melt fraction on the deformation behaviour of peridotite. Earth Planet. Sci. Lett. 246, 177–187. doi:10.1016/j.epsl.2006.04.027.
Secco, R.A., Rutter, M.D., Balog, S.P., Liu, H., Rubie, D.C., Uchida, T., Frost, D., Wang, Y., Rivers, M., Sutton, S.R., 2002. Viscosity and density of Fe–S liquids at high pressures. J. Phys. Condens. Matter 14, 11325–11330.
Stevenson, D.J., 1990. Fluid dynamics of core formation. In: Newsom, H.E., Jones, J.H. (Eds.), Origin of the Earth. Oxford Univ. Press, Houston, pp. 231–249.
Stewart, A.J., Schmidt, M.W., van Westrenen, W., Liebske, C., 2007. Mars: a new core crystallization regime. Science 316, 1323–1325.
Sumita, I., Yoshida, Sh., Kumazawa, M., Hamano, Y., 1996. A model for sedimentary compaction of a viscous medium and its application to inner core growth. Geophys. J. Int. 124, 502–524.
Taylor, G.J., 1992. Core formation in asteroids. J. Geophys. Res. 97 (E9), 14717–14726.
Terasaki, H., Frost, D.J., Rubie, D.C., Langenhorst, F., 2007. Interconnectivity of Fe–O–S liquid in polycrystalline silicate perovskite at lower mantle conditions. Phys. Earth Planet. Inter. 161, 170–176. doi:10.1016/j.pepi.2007.01.011.
Terasaki, H., Frost, D.J., Rubie, D.C., Langenhorst, F., 2008. Percolative core formation in planetesimals. Earth Planet. Sci. Lett. doi:10.1016/j.epsl.2008.06.019.
Terasaki, H., Urakawa, S., Funakoshi, K., Nishiyama, N., Wang, Y., Nishida, K., Sakamaki, T., Suzuki, A., Ohtani, E., 2009. In situ measurements of interfacial tension of Fe–S and Fe–P liquids under high pressure using X-ray radiography and tomography techniques. Phys. Earth Planet. Inter. doi:10.1016/j.pepi.2009.01.004.
Tonks, W.B., Melosh, H.J., 1992. Core formation by giant impacts. Icarus 100, 326–346.
Urakawa, S., Terasaki, H., Funakoshi, K., Kato, T., Suzuki, A., 2001. Radiographic study on the viscosity of the Fe–FeS melts at the pressure of 5 to 7 GPa. Am. Mineral. 86 (4), 578–582.
Usselman, T.M., 1975. Experimental approach to the state of the core: part I. The liquidus relations of the Fe-rich portion of the Fe–Ni– S system from 30 to 100 kbar. Am. J. Sci. 275, 278–290.
Wade, J., Wood, B.J., 2005. Core formation and the oxidation state of the Earth. Earth Planet. Sci. Lett. 236, 78–95. doi:10.1016/j.epsl.2005.05.017.
Walte, N.P., Becker, J.K., Bons, P.D., Rubie, D.C., Frost, D.J., 2007. Liquid-distribution and attainment of textural equilibrium in a partially-molten crystalline system with a high-dihedral-angle liquid phase. Earth Planet. Sci. Lett. 262, 517–532. doi:10.1016/j.epsl.2007.08.003.
Walter, M.J., 2003. Melt extraction and Compositional Variability in Mantle Lithosphere. Treatise in Geochemistry. Elsevier, pp. 363–394. Chapter 2.08.
Walter, M.J., Tronnes, R.J., 2004. Early Earth differentiation. Earth Planet. Sci Lett. 225, 253–269.
Wetherill, G.W., 1975. Radiometric chronology of the early solar system. Annu. Rev. Nuc. Sci. 25, 283–328.
Wood, B.J., Halliday, A.N., 2005. Cooling of the Earth and core formation after the giant impact. Nature 437 (27), 1345–1348. doi:10.1038/nature04129.
Wood, B.J., Walter, M.J., Wade, J., 2006. Accretion of the Earth and segregation of its core. Nature 441, 825–833. doi:10.1038/nature04763.
Yang, X.-s., 2001. Density driven compactional flow in porous media. J. Comput. Appl. Math. 130, 245–257.
Yoshino, T., Watson, E.B., 2005. Growth kinetics of FeS melt in partially molten peridotite: an analogue for core-forming processes. Earth Planet. Sci. Lett. 235, 453–468. doi:10.1016/j.epsl.2005.04.021.
Yoshino, T., Walter, M.J., Katsura, T., 2003. Core formation in planetesimals triggered by permeable flow. Nature 422, 154–157. doi:10.1038/nature01459.
Yoshino, T., Walter, M.J., Katsura, T., 2004. Connectivity of molten Fe alloy in peridotite based on in situ electrical conductivity measurements: implications for core formation in terrestrial planets. Earth Planet. Sci. Lett. 222, 625–643. doi:10.1016/j.epsl.2004.03.010.
Zimmerman, M.E., Kohlstedt, D.L., 2004. Rheological properties of partially molten lherzolite. J. Petrol. 45, 275–298.